

A Seismic Data Compression System Using Subband Coding

A. B. Kiely and F. Pollara
Communications Systems Research Section

This article presents a study of seismic data compression techniques and a compression algorithm based on subband coding. The algorithm includes three stages: a decorrelation stage, a quantization stage that introduces a controlled amount of distortion to allow for high compression ratios, and a lossless entropy coding stage based on a simple but efficient arithmetic coding method. Subband coding methods are particularly suited to the decorrelation of nonstationary processes such as seismic events. Adaptivity to the nonstationary behavior of the waveform is achieved by dividing the data into separate blocks that are encoded separately with an adaptive arithmetic encoder. This is done with high efficiency due to the low overhead introduced by the arithmetic encoder in specifying its parameters. The technique could be used as a progressive transmission system, where successive refinements of the data can be requested by the user. This allows seismologists to first examine a coarse version of waveforms with minimal usage of the channel and then decide where refinements are required. Rate-distortion performance results are presented and comparisons are made with two block transform methods.

I. Introduction

A typical seismic analysis scenario involves collection of data by an array of seismometers, transmission over a channel offering limited data rate, and storage of data for analysis. Seismic data analysis is performed for monitoring earthquakes and for planetary exploration, as in the planned study of seismic events on Mars. Seismic data compression systems are required to cope with the transmission of vast amounts of data over constrained channels and must be able to accurately reproduce both low-energy seismic signals and occasional high-energy seismic events.

We describe a compression algorithm that includes three stages: a decorrelation stage based on subband coding, a uniform quantization stage, and a lossless entropy coding stage based on arithmetic coding. Rate-distortion performance results are presented and comparisons are made with two block transform methods: the discrete cosine transform (DCT) and the Walsh-Hadamard transform (WHT).

Subband coding methods are particularly suited to the decorrelation of nonstationary processes such as seismic events. For most seismic data, signal energy is more concentrated in the low-frequency subbands, which suggests the use of nonuniform subband decomposition. The decorrelation stage is implemented by quadrature mirror filters using a lattice structure. Adaptivity to the nonstationary behavior of the waveform is achieved by dividing the data into blocks that are separately encoded.

Appendix B

Performance of the CSC Correlator

The method of estimating the relative signal phases for complex-symbol combining is analogous to the full-spectrum combining algorithm; using the extra correlation to compensate for the noise bias, the complex correlation can be expressed as

$$\begin{aligned}
 Z &= \frac{1}{N} \sum_{k=1}^N \tilde{Y}_1(k) \tilde{Y}_i^*(k) - \frac{1}{N} \sum_{k=1}^N \tilde{N}_1(k) \tilde{N}_i^*(k) \\
 &= \sqrt{P_{D_1} P_{D_i}} \overline{C_{sc_1}} \overline{C_{sy_1}} \overline{C_{sc_i}} \overline{C_{sy_i}} e^{j\phi_{1i}} + \frac{1}{N} \sum_{k=1}^N \sqrt{P_{D_1}} C_{sc_1} C_{sy_1} e^{j\theta_1} \tilde{N}_i^*(k) \\
 &\quad + \frac{1}{N} \sum_{k=1}^N \sqrt{P_{D_i}} C_{sc_i} C_{sy_i} e^{-j\theta_i} \tilde{N}_1^*(k) + \frac{1}{N} \sum_{k=1}^N \tilde{N}_1(k) \tilde{N}_i^*(k) - \frac{1}{N} \sum_{k=1}^N \tilde{N}_1'(k) \tilde{N}_i'^*(k) \\
 &= \sqrt{P_{D_1} P_{D_i}} \overline{C_{sc_1}} \overline{C_{sy_1}} \overline{C_{sc_i}} \overline{C_{sy_i}} e^{j\phi_{1i}} + \tilde{N} \tag{B-1}
 \end{aligned}$$

where N is the number of symbols averaged over, given by $N = T_{corr}/T_{sym}$, and the noise term \tilde{N} has zero mean. The statistics of this noise can be analyzed in the same manner as before; here, the effective correlation bandwidth for both the lowpass and the bandpass correlation is $R_{sym}/2$. Using the definition given by Eq. (32), the correlator SNR can be shown to be equal to

$$SNR_{corr,csc} = \frac{P_{D_1}}{N_{o_1}} \frac{T_{corr} \overline{C_{sc_1}}^2 \overline{C_{sy_1}}^2 \overline{C_{sc_i}}^2 \overline{C_{sy_i}}^2}{\overline{C_{sc_i}}^2 \overline{C_{sy_i}}^2 + \overline{C_{sc_1}}^2 \overline{C_{sy_1}}^2 (1/\gamma_i) + (N_{o_i}/P_{D_i}) 2R_{sym}} \tag{B-2}$$

The density function for the phase estimation error can be found in a manner analogous to that applied in Appendix A. The only difference is in the expression for the correlator SNR; otherwise, both problems are inherently governed by the same mathematics. The density function for the phase estimation error $\Delta\phi_{1i}$ is thus given by Eq. (A-15), with $SNR_{corr,fs}$ replaced by $SNR_{corr,csc}$.

The compression technique described in this article can be used as a progressive transmission system, where successive refinements of the data can be requested by the user. This allows reconstruction of a low-resolution version of the waveform after receiving only a small portion of the compressed data. This could allow seismologists to make a preliminary examination of the waveform with minimal usage of the channel and then decide where high-resolution refinements are desired.

In general, given a fixed transmission rate, lossy compression algorithms applied to high-accuracy instruments deliver higher scientific content than lossless compression methods applied to lower accuracy instruments.

II. Subband Decomposition

In the analysis stage of subband coding, a signal is filtered to produce a set of subband components, each having smaller bandwidth than the original signal. Because of this limited bandwidth, each component is downsampled, so that the subband transformed data contain as many data points as the original signal. The subband components are then quantized and compressed. In the synthesis stage, the reconstructed signal is formed by adding together the subbands obtained by applying the inverse filters to upsampled versions of the subband components.

The analysis and synthesis filters used here are finite impulse response (FIR) quadrature mirror filters (QMF) implemented using the lattice structures shown in Figs. 1 and 2, which are described in [7,1]. Analysis and synthesis quadrature mirror filters of order $2M$ are implemented using an M -stage lattice structure. Suitable lattice filters can be found in [1, p. 267] and [7, p. 310].

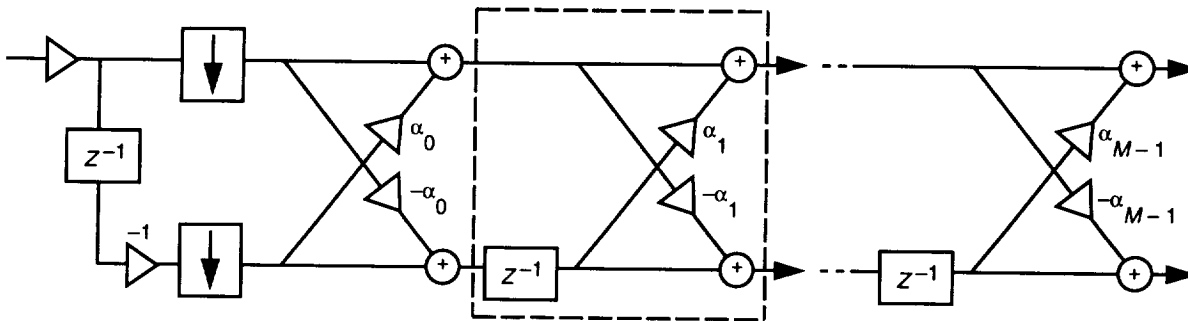


Fig. 1. Analysis filter structure. (The stage inside the box is repeated.)

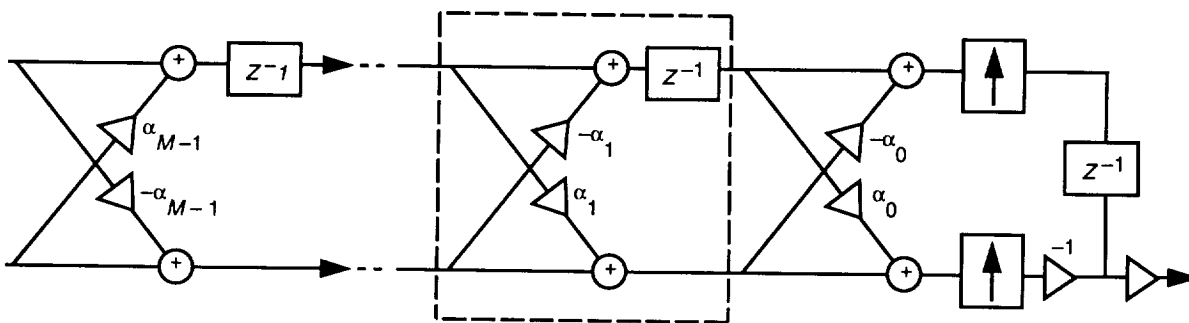


Fig. 2. Synthesis filter structure.

For most seismic data samples, signal energy is concentrated primarily in the low subbands.¹ Figures 3 and 4 give two periodograms (power spectral density estimates [4]) for seismic data. The uneven distribution of spectral energy in seismic signals provides the basis for subband coding source-compression techniques. For effective signal coding, subspectra containing more energy deserve higher priority for further processing.

A subband decomposition that tends to work well for seismic data is the dyadic tree decomposition shown in Fig. 5. The signal is first split into low- and high-frequency components in the first level. A two-band subband decomposition uses high-pass and low-pass digital filters to decompose a data sequence into high (H) and low (L) subbands, each containing half as many points as the original sequence. The filter is repeated to further decompose the low subband. This process may be repeated several levels.

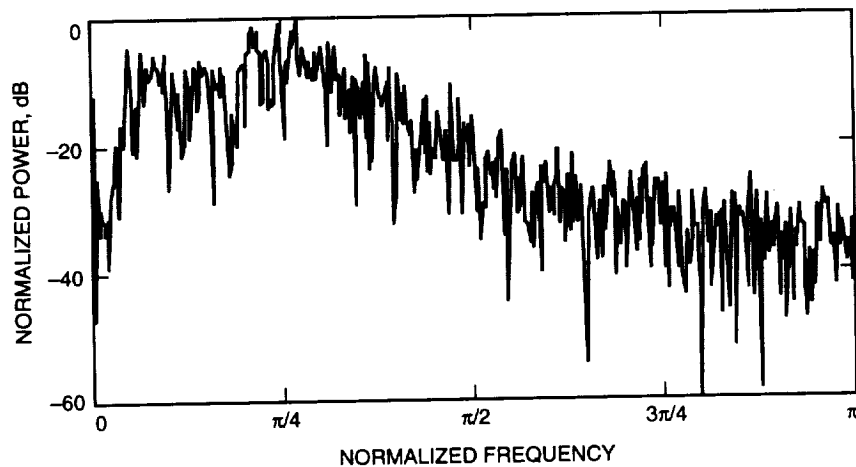


Fig. 3. Periodogram of 1024-point EHZ (100 samples/s) data sample containing seismic event.

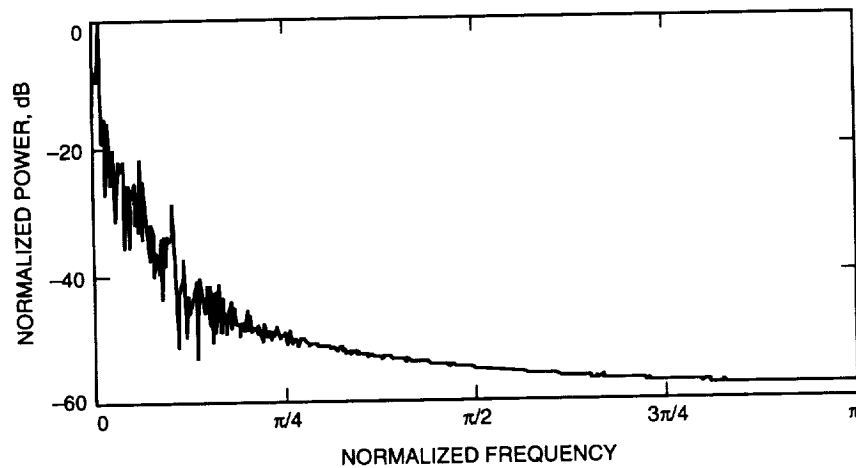


Fig. 4. Periodogram of 1024-point BHZ (20 samples/s) data sample containing seismic event.

¹ This generally applies to the event (EHZ) and broadband (BHZ) seismic data components, which have sample rates of 100 and 20 samples/s, respectively. Energy in long-period (LHZ) data, which has a sample rate of only 1 sample/s, is typically not as concentrated in the low frequencies. However, because of the much lower sample rate, compression of this component is not as important as the others. A different subband decomposition could be implemented to accommodate this type of data.

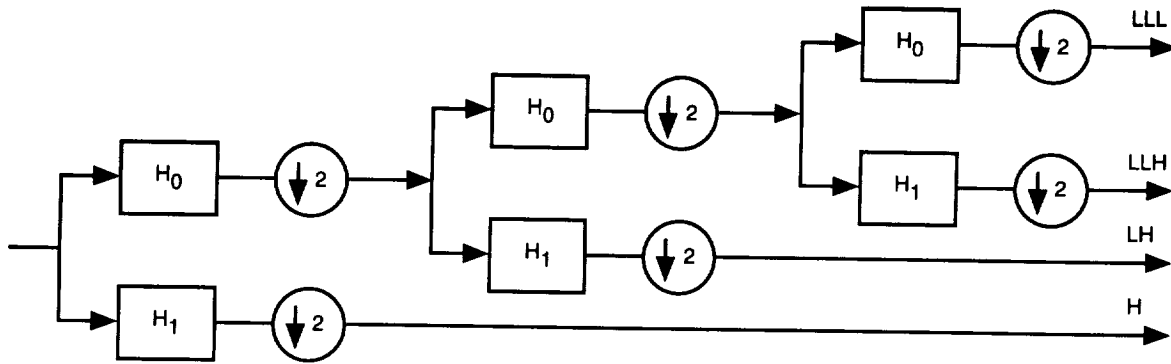


Fig. 5. Subband decompositions.

Increasing the number of subbands produces diminishing rate-distortion returns, with gains often observable only at very high compression ratios. One reason for this is that, after several decompositions, the energy is no longer so highly concentrated in the lowest subband.

So that a filtered block has the same length as the original, each block is periodically extended (i.e., repeated in time) before filtering, and the components corresponding to a single period of the filtered extended signal are taken as the filtered signal. If this operation were not performed, the length of the filtered signal would exceed the original block length. An unfortunate side effect of periodic extension is that it often produces high-frequency components at the edges of data blocks, an effect whose impact increases with filter length. These components are not as easily compressed as the rest of the subband data and are separated for compression purposes. Longer filters are also more likely to introduce noticeable spurious effects at the onset of a high-energy seismic event, as we shall see in Section VI. It is also worth noting that longer filters generally do not dramatically outperform shorter filters, as we will see in the following section.

III. Comparing Subband Coding to Block Transforms

For comparison purposes, we also examined the discrete cosine transform (DCT), a popular technique used in the compression of two-dimensional data (e.g., images). A general description of the DCT as used in the Joint Photographic Experts Group (JPEG) compression algorithm can be found in [5, pp. 113–128]. The DCT can also be applied to one-dimensional data, as is done here.

The data are partitioned into blocks of length 8, the DCT of each block is computed using the 8×8 DCT matrix, and these transformed values are uniformly quantized. A different quantizer step size could be used for each coefficient, but in practice, for most seismic data samples, near-optimum performance is obtained when all quantizers use the same step size. The quantized coefficients are arranged in groups of 8 blocks for subsequent coding, so that 64 transformed coefficients are encoded at a time. In this way, the procedure is similar to a one-dimensional version of the JPEG algorithm. The lowest frequency (dc) quantized coefficients are encoded using differential pulse-code modulation (DPCM) and Huffman coding, except at very low rates, when a run-length code is used. The remaining (ac) coefficients are run-length encoded, in order of increasing frequency. The run-length encoding used is the same as that described in [5, pp. 114–115].

We also used the same algorithm with an 8×8 WHT in place of the DCT, separately encoding each coefficient. The WHT performed uniformly worse (see Fig. 6). To make a fair comparison with subband coding, we compared the block transform compression methods to subband coding combined with Huffman coding of the quantizer output, rather than the arithmetic coding procedure to be described in the next section.

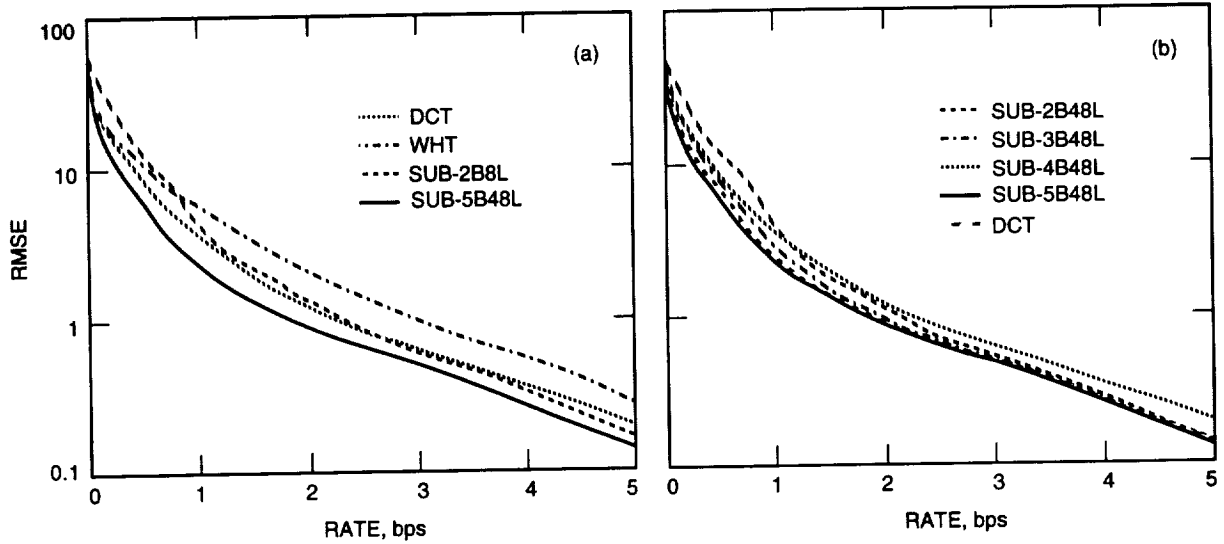


Fig. 6. Rate-distortion performance for various compression techniques applied to a seismic data sample: (a) comparison with block transform methods and (b) comparison of different subband decompositions.

Rate-distortion curves for a seismic data sample using these different techniques are shown in Fig. 6. The labels on the curves corresponding to subband coding identify the number of subbands and the particular filters used. For example, “3B8L” refers to a three-band decomposition using an order-8 FIR filter. In terms of root-mean-square error (RMSE), subband coding is able to outperform the DCT and WHT with only moderate complexity.

IV. Entropy Coding Stage: Arithmetic Coding

Anyone who has experienced an earthquake knows that the energy present in a seismic signal can vary tremendously over time. Consequently, seismometers have a large dynamic range, and it is desirable to have an adaptive compression system capable of transmitting low-energy and high-energy signals reliably.

A block of m data samples produces m subband coded samples. Because of the downsampling operation, half of these are high-subband samples, one-fourth are low-high-subband samples, etc. All of the samples from a particular subband are quantized and encoded together block adaptively. Because this is a block-to-block encoding procedure, the effects of a channel error are confined to the block during which that error occurs. The block encoding provides the additional benefit of adaptivity.

The output of the subband coding stage is a sequence of real numbers that are quantized and then compressed. For seismic data, as with many other types of data, these components are generally zero-mean, roughly symmetric, and have a probability density that is decreasing as we move away from the origin. This is illustrated in Fig. 7, which gives an empirical probability density function (pdf) of signal amplitude from a low-pass-filtered seismic data sample.

The compression scheme we use is bit-wise arithmetic coding [2]. A high-resolution quantizer is used, and the quantized values are mapped into fixed-length binary codewords. Figure 8 illustrates the bit assignment for a four-bit quantizer: The first bit indicates the sign of the quantizer reconstruction point, and each successive bit gives progressively higher resolution information. Because the pdf is zero mean and decreasing as we move away from the origin, a zero will be more likely than a one in every bit position. This redundancy is exploited using a binary arithmetic encoder to achieve compression.

V. Progressive Transmission Behavior

In designing a compression system to be used in progressive transmission or in situations where rate constraints may result in the loss of data, it is important to consider the rate-distortion behavior of the system when only portions of the compressed data have been received. Such performance can be improved simply by careful choice of the order in which the compressed data are transmitted.

The typical characteristics of subband-filtered seismic data motivate our transmission strategy. Because the probability density for subband-filtered seismic data is generally zero mean (see Fig. 7), the sign bit layers of each subband usually have high entropy. Because the energy in seismic waveforms is often quite small, the high-order bit layers (excluding the sign bit) often consist entirely of zeros or can be readily compressed using the block-adaptive arithmetic encoder. Finally, as mentioned in Section II, periodic extension of the data is required in the subband filtering stage, which often produces high-frequency components at the start of data segments. These initial values, which we call transients, are encoded separately from the rest of the data. All but the lowest subband contain these transients.

Generally speaking, we transmit compressed data ordered from the most significant bit layer to the least significant bit (LSB) layer, and within this order, proceeding from the lowest frequency to the highest frequency subband. Initially, we skip the sign bit layer and begin with the next most significant bit layer. If this layer consists entirely of zeros (which is usually the case), a single “0” is transmitted and we move on to the same layer in the next higher subband. For every subband, a “0” is transmitted for each layer consisting entirely of zeros until a “1” is transmitted at some layer ℓ , denoting that the ℓ th layer is not all zeros. At this point, we transmit the sign bits (using the block-adaptive arithmetic coding procedure already described). Then the transients for the subband are transmitted using run-length encoding of the leading zeros, and then the (compressed) ℓ th bit layer is transmitted. Then we proceed to the ℓ th layer for the next higher subband. Each subsequent bit layer of the subband is sent, compressed by arithmetic coding.

Because the order of transmission is determined using a rather simple decision procedure, the additional overhead required to describe the transmission order is quite small—it consists only of occasional one-bit flags. As an example, Fig. 9 shows a seismic data sample along with waveforms reconstructed from only small portions of compressed data for a 51.2-s (1024-point) block.

The rate-distortion progressive transmission performance of this system for one seismic data sample can be seen in Fig. 10. The highest rate point of each curve is the final design goal, and the rest of the curve shows the rate-distortion performance when the signal is reconstructed using only portions of the data. It is remarkable that the curves are nearly indistinguishable. Note that a system designed to transmit at a rate of 5 bits per sample (bps) but cut off at only 2.5 bps performs almost as well as a system designed to operate at 2.5 bps.

VI. Distortion Measures and Artifacts

In the previous sections, we have been mostly concerned with the mean-square error (MSE) distortion measure. However, mean-square distortion may not be a sufficient indicator of fidelity for seismic analysis purposes. For example, Spanias et al. [6] examined the effect of transform data compression methods on estimation of the body wave magnitude, which they call “the key parameter used in seismic analysis.” Other distortion measures may be more relevant, depending on the interests of the seismologists who will ultimately analyze the data. Unfortunately, we do not know of a distortion measure that seismologists will widely accept as the most useful.

Artifacts are erroneous features that may appear in the reconstructed waveform. Different algorithms create different artifacts depending on their modes of operation. For example, “blockiness” is an artifact commonly associated with block transforms such as the DCT, while “ringing” may be produced by

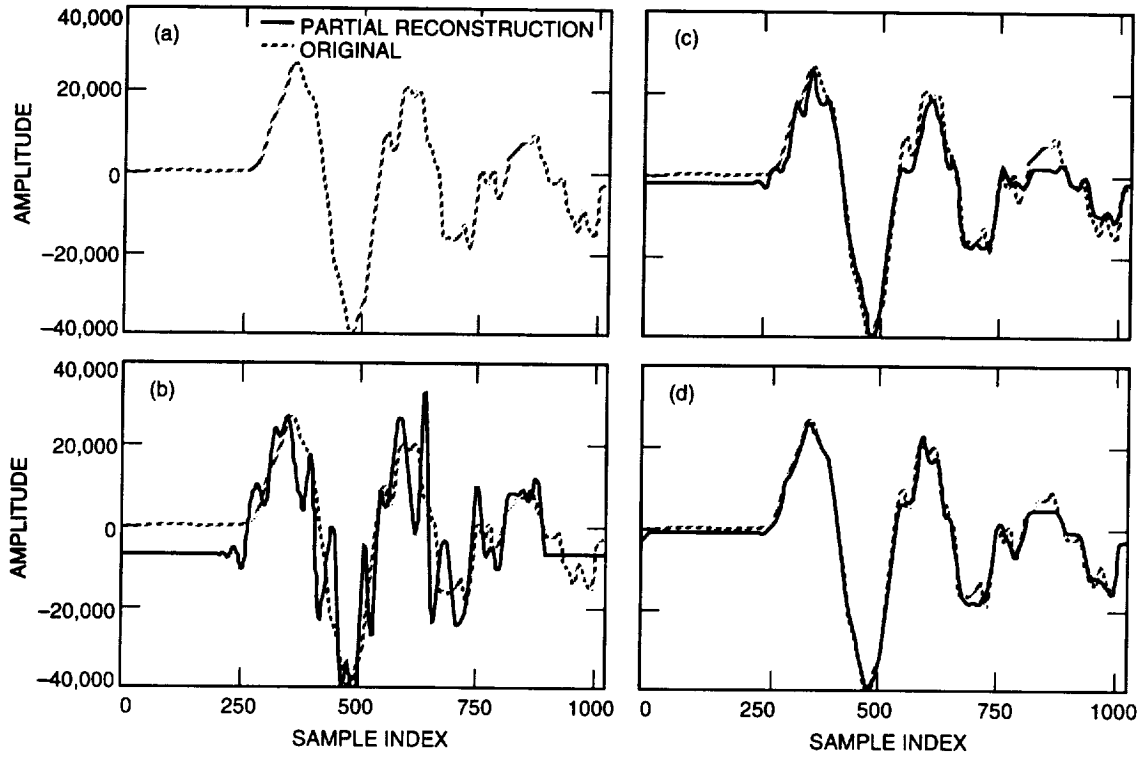


Fig. 9. Progressive transmission example: (a) original, (b) 0.1 bps, (c) 0.2 bps, and (d) 0.3 bps.

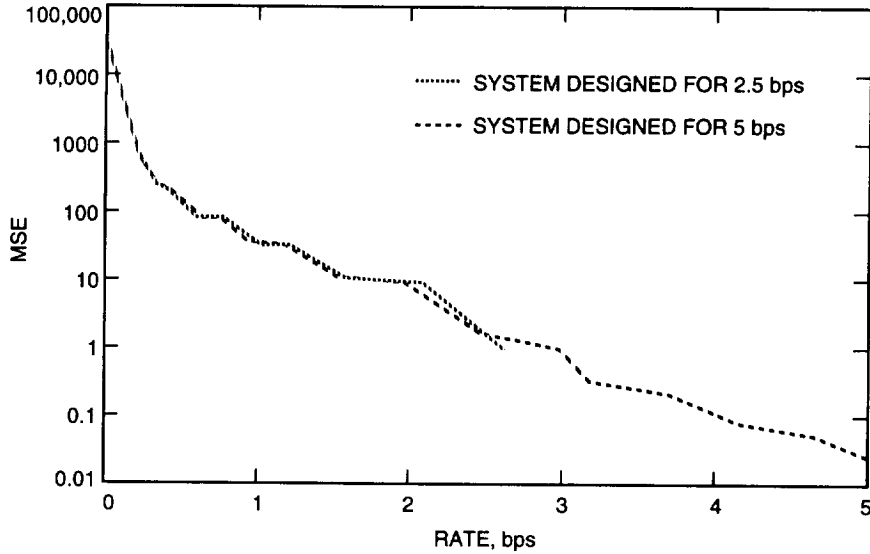


Fig. 10. Progressive transmission performance.

subband coding using a filter with a too sharp response. Even a given algorithm may exhibit different artifacts depending on the bit rate at which it is operated. Some artifacts may be more objectionable than others for correct waveform interpretation.

In this section, we illustrate two artifacts that may be observable in subband coding depending on the mode of operation and the compression ratio. Understanding the causes and cures for such artifacts

allows seismologists to give meaningful feedback to engineers in deciding what features of a compression system are most important.

We are actively trying to engage the seismology community to characterize any essential artifacts produced by the proposed method [8]. One of the results of this interaction was the objection of seismologists to the precursor artifact created by a particular subband filter, as shown in Fig. 11(b). After determining that such an artifact was due to a filter with a too sharp response, we experimented with different, shorter filters, producing the result shown in Fig. 11(c), which reduces the precursor problem while preserving essentially the same compression ratio.

A different artifact is introduced when the quantizer step size is quite large (this equivalent effect may occur if the waveform is reconstructed using only a portion of the data). In this case, each subband will have low resolution, and because most of the energy is contained in the low frequencies, the high-frequency subbands may all be zeroed out. This may produce the interesting smoothing effect that can be observed in the periodogram of the reconstructed waveform shown in Fig. 12. If this frequency range has more significance than the others, the corresponding subbands could be assigned higher priority in the transmission and quantization stages.

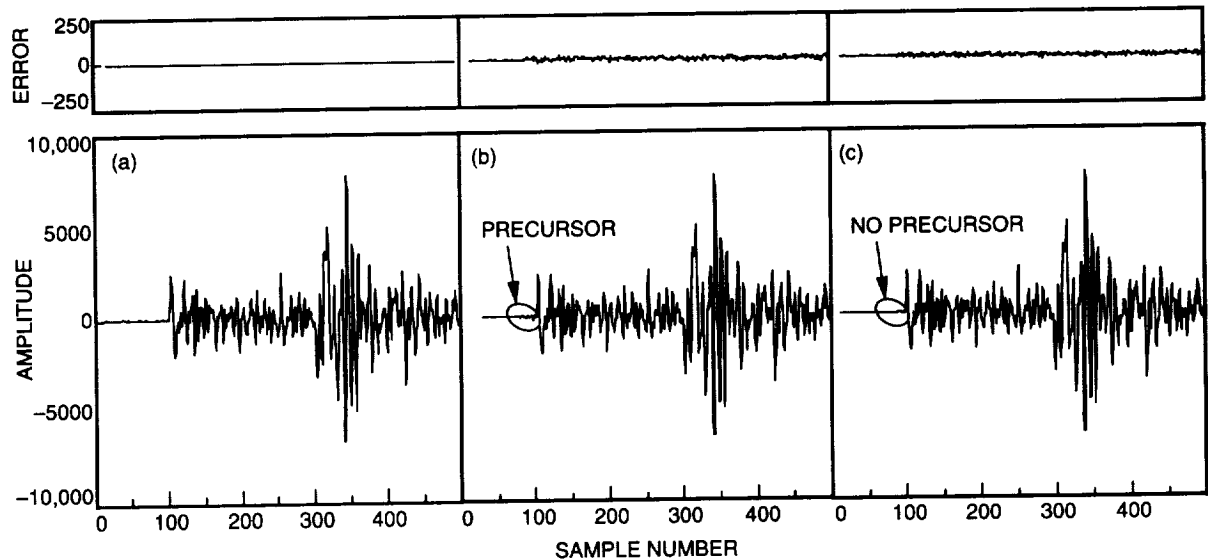


Fig. 11. Original and reconstructed waveforms for two different filters: (a) original, 24 bps, (b) reconstructed, 0.8 bps, and (c) reconstructed, 0.8 bps (improved filter).

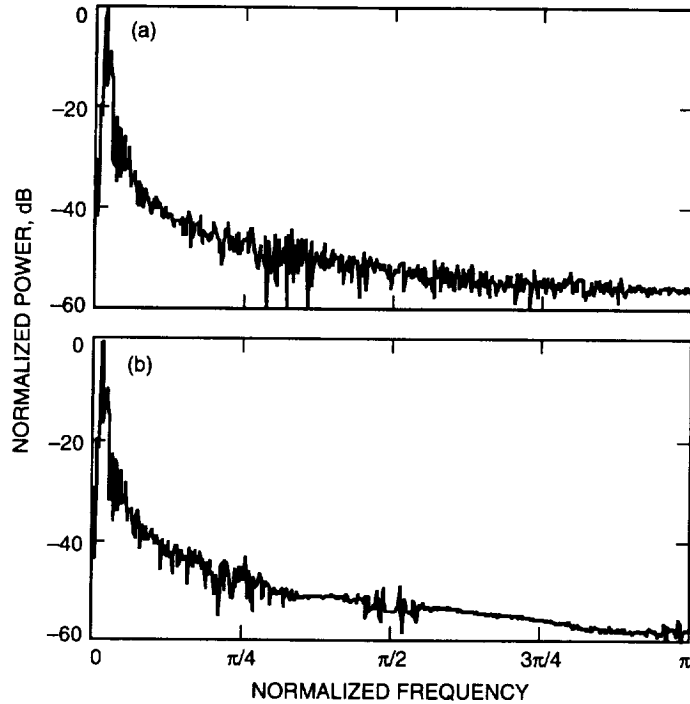


Fig. 12. Periodograms of 1024-point BHZ (20 samples/s) background (i.e., nonevent) data constructed from (a) the original and (b) the reconstructed waveform with low-resolution quantizer.

References

- [1] A. N. Akansu and R. A. Haddad, *Multiresolution Signal Processing*, San Diego California: Academic Press, 1992.
- [2] A. B. Kiely, "Bit-Wise Arithmetic Coding for Data Compression," *The Telecommunications and Data Acquisition Progress Report 42-117, January-March 1994*, Jet Propulsion Laboratory, Pasadena, California, pp. 145-160, May 15, 1994.
- [3] R. J. McEliece and T. H. Palmatier, "Estimating the Size of Huffman Code Preambles," *The Telecommunications and Data Acquisition Progress Report 42-114, April-June 1993*, Jet Propulsion Laboratory, Pasadena, California, pp. 90-95, August 15, 1993.
- [4] A. V. Oppenheim and R. W. Schaffer, *Digital Signal Processing*, Englewood Cliffs, New Jersey: Prentice-Hall, 1975.
- [5] M. Rabbani and P. W. Jones, *Digital Image Compression Techniques*, Bellingham, Washington: SPIE Press, 1991.
- [6] A. S. Spanias, S. B. Jonsson, and S. D. Stearns, "Transform Methods for Seismic Data Compression," *IEEE Trans. Geoscience and Remote Sensing*, vol. 29, no. 3, pp. 407-416, May 1991.
- [7] P. P. Vaidyanathan, *Multirate Systems and Filter Banks*, Englewood Cliffs, New Jersey: PTR Prentice-Hall, 1993.
- [8] *Workshop on the Use of Data Compression in Seismic Data Proceedings*, Jet Propulsion Laboratory, Pasadena, California, March 2, 1994.

DSS-24 Microwave Holography Measurements

D. J. Rochblatt, P. M. Withington, and H. J. Jackson
Ground Antennas and Facilities Engineering Section

The JPL DSN Microwave Antenna Holography System (MAHST) was applied to the newly constructed DSS-24 34-m beam-waveguide antenna at Goldstone, California. The application of MAHST measurements and corrections at DSS 24 provided the critical RF performance necessary to not only meet the project requirements and goals, but to surpass them. A performance increase of 0.35 dB at X-band (8.45 GHz) and 4.9 dB at Ka-band (32 GHz) was provided by MAHST, resulting in peak efficiencies of 75.25 percent at X-band and 60.6 percent at Ka-band (measured from the Cassegrain focus at f1). The MAHST enabled setting the main reflector panels of DSS 24 to 0.25-mm rms, making DSS 24 the highest precision antenna in the NASA/JPL DSN. The precision of the DSS-24 antenna (diameter/rms) is 1.36×10^5 , and its gain limit is at 95 GHz.

I. Introduction

The JPL Microwave Antenna Holography System (MAHST) (Fig. 1) [1] has become the leading technique for increasing the performance of the large NASA/JPL DSN antennas, especially at the shorter wavelengths (X-band (8.45 GHz) and Ka-band (32 GHz)). The MAHST provides an efficient and low-cost technique to optimize and maintain the performance and operation of the large DSN antennas, providing far-field amplitude and phase pattern measurement with a 90-dB dynamic range, and enabling high-resolution and high-precision antenna imaging with a standard deviation of 100 μm . The panel setting/unbending screw adjustment is provided with an accuracy of 10 to 20 μm . Fast subreflector position optimization is provided, which increases the antenna performance capacity and pointing accuracy. The MAHST is a portable system that can be shipped to any DSN antenna around the world and can be easily interfaced with its encoders and antenna drive systems. The MAHST was designed utilizing many off-the-shelf commercially available components. The remaining parts were designed and built at JPL. The MAHST has been successfully tested and demonstrated at the NASA/JPL DSN [1,2].

The microwave holography technique utilizes the Fourier transform relationship between the complex far-field radiation pattern of an antenna and the complex aperture field distribution. Resulting aperture phase and amplitude distribution data are used to derive various crucial performance parameters, including panel alignment, subreflector position, antenna aperture illumination, directivity at various frequencies, and gravity deformation effects [3,4]. Strong continuous wave (CW) signals obtained from geostationary satellite beacons are utilized as far-field sources. Strong CW beacon signals are available on nearly all satellites at Ku-band (10.7 to 12.7 GHz), X-band (7.0 to 7.8 GHz), and C-band (3.7 to 4.2 GHz). A portable 2.8-m reference antenna (Fig. 1) is used as a phase reference and provides the signal to the receiver phase-lock-loop (PLL) channel. The intermediate-frequency (IF) section of a Hewlett Packard Microwave Receiver (HP8530A) and an external JPL-designed and -built PLL enable